


Characterization and mapping of MIS-2 thermal contraction crack polygons in Western Transdanubia, Hungary

Beáta Farkas¹  | György Sipos² | Tamás Bartyik² | Edina Józsa¹ | Szabolcs Czigány³ | Richárd Balogh¹ | Gábor Varga³ | János Kovács^{3,4} | Szabolcs Ákos Fábrián³

¹Doctoral School of Earth Sciences, University of Pécs, Pécs, Hungary

²University of Szeged, Faculty of Science and Informatics, Institute of Geosciences, Szeged, Hungary

³University of Pécs, Faculty of Sciences, Institute of Geography and Earth Sciences, Pécs, Hungary

⁴University of Pécs, Szentágotthai Research Centre, Environmental Analytical and Geoanalytical Research Group, Pécs, Hungary

Correspondence

Beáta Farkas, University of Pécs, Doctoral School of Earth Sciences, Pécs, Hungary.
Email: fbea97@gamma.ttk.pte.hu

Abstract

The Pannonian Basin was located in the southernmost, disputed limit of permafrost during the Last Glacial Maximum (LGM). In the western part of the basin, over an area of 1,200 km², more than 150 sites with polygonal patterned ground were surveyed, and 72 sediment samples from forms identified as relict sand wedges were collected. Ten optically stimulated luminescence ages were obtained from the infills, while morphometric analyses were also carried out on satellite images. Our study revealed that the polygonal networks developed in several phases, from 15.01 ± 1.68 to 23.0 ± 1.7 ka. The polygons have an average diameter of 13–23 m and are mainly present on flat surfaces, intruding into the gravelly, alluvial host of the paleo-Rába. Statistical analyses highlighted the short transportation period of the sandy infill and multiple sediment provenances. This study adds further data to assess the presence of permafrost or deep seasonal frost and to the interpretation of the LGM in the central European periglacial domain.

KEYWORDS

cropmarks, grain size analysis, OSL, Pannonian Basin, remote sensing, sand wedges

1 | INTRODUCTION

Networks of polygonal cracks in soils can be developed in various environments on Earth. They can be formed due to frost action, desiccation, or even pedogenic processes.^{1–3} Investigation of these features offers valuable insight into past paleoenvironmental changes as well as recent surface processes. This paper, however, only deals with polygonal networks derived from ground thermal contraction. This process occurs when decreasing temperatures in the frozen ground generate tensile stresses greater than the tensile strength of the ground. Such stresses are favored by both rapid cooling and low temperature,^{4,5} and therefore polygonal cracks related to thermal contraction are present in both recent (e.g., Watanabe et al,⁶ Wolfe et al⁷)

and relict (Rodríguez-López et al,⁸ Ewertowski et al⁹ and references therein) periglacial environments. Polygons originating from thermal contraction cracking in frozen ground are one of the most well-recognized and widespread landforms in permafrost-controlled lowlands.¹⁰ According to the remote sensing investigations of Ewertowski et al,⁹ seven types of relict polygonal networks can be distinguished, based on their diameters, regularities, and intersecting angles.

Thermal contraction cracks are of numerous types based on their infilling material (e.g., ice, sand, ground, composite) and their chronological status (active or relict forms). Primary and secondary structures need to be distinguished within the term “sand wedge.” When the wedge-shaped cracks are filled exclusively with allochthonous sand during their lifetime, they are called primary structures.^{11,12} Former, melted ice

This is an open access article under the terms of the [Creative Commons Attribution](https://creativecommons.org/licenses/by/4.0/) License, which permits use, distribution and reproduction in any medium, provided the original work is properly cited.

© 2023 The Authors. *Permafrost and Periglacial Processes* published by John Wiley & Sons Ltd.

wedges that are later filled with sand are called secondary structures.¹³ If inactive, the wedges are referred to as relict sand wedges.¹⁴

The distribution of the above-mentioned past periglacial features has been mapped in most of western and central Europe, but the identification and paleoenvironmental significance of such features remain uncertain.^{7,14}

Based on environmental proxies (i.e., ice wedge pseudomorphs, composite pseudomorphs, sand wedges, cryoturbations, etc.), previous studies have tried to establish the spatial extent/zones of permafrost types within the Pannonian Basin during the Last Glacial Maximum (LGM).¹⁵ Although some early reconstructions proposed that almost the entire basin was affected by permafrost,^{16–19} these estimations did not distinguish between permafrost types. Later, Vandenberghe et al,¹⁵ based on existing archival data, established a map of the Last Permafrost Maximum permafrost extent in the Northern Hemisphere. Caution must be exercised because there are limitations to these reconstructions, such as the topographical influence on climate-controlled permafrost, as stated by Ruzsiczay-Rüdiger and Kern.²⁰ At that time, however, sand wedges found in France were considered indicative of continuous permafrost, because active sand wedges were only known from Antarctica. Since then, Wolfe et al⁷ have described active sand wedges in deep seasonal frost in Canada, providing some support to the idea that the French Pleistocene sand wedges south of 47.5°N developed in a permafrost-free context as Andrieux et al^{21,22} had already suggested.

Landforms related to periglacial processes were described in the 20th century in the Pannonian Basin.^{23–27} Recently, cryogenic features were further investigated by Fábrián et al²⁸ and Kovács et al²⁹ In these papers, the authors determined the age of the infilling material for the Mogyoród site. Optically stimulated luminescence (OSL) dating has shown that thermal contraction cracks were filled with allochthonous sediments during Marine Isotope Stage (MIS) 2.²⁸ Knowledge regarding the dating of their formation is essential for paleoclimatic reconstructions. Luminescence dating on relict primary and secondary sand wedges (ice wedge pseudomorphs) have been published by several authors.^{13,22,30–35}

In recent decades, only a few studies have investigated the grain size distribution (GSD) of relict sand wedge infillings.^{11–13,35–39} Primary infillings—according to the papers cited above—are commonly well sorted, allochthonous sandy deposits, which indicates a cold environment with strong eolian activity. In Hungary, grain size analysis of relict sand wedge infillings is lacking. However, other evidence of former intensive wind activity has already been detected.^{40,41}

This paper describes the characteristics of polygonal patterned ground in the Kemeneshát region, western Transdanubia, discusses the main sedimentological properties of the infilling material, and proposes a time-frame for their formation based on OSL dating.

2 | STUDY AREA

The analysis was performed on a regional scale, over the Lower and Higher Kemeneshát microregions in the western part of Transdanubia, Hungary (Figure 1).

Kemeneshát was located ca. 600 km from the maximum southern limit of the Fennoscandian Ice Sheet (FIS) during the LGM (26.5–19 ka⁴²). After retreat of the ice sheet, at its smallest extent (15 ka), this distance increased to 900 km.

The study site is located in an area bounded by three rivers (River Rába, Marcal and Zala), and covers nearly 1,200 km². The mean elevation of the Kemeneshát region is 190–250 m a.s.l. The area is built up of late Miocene (Pannonian) lacustrine clays and Pliocene cross-bedded fluvial sand, and this Neogene basement is overlain by 20–25-m-thick gravel deposits of the Rába river from the Lower and Middle Pleistocene.⁴³ Cryoturbation structures were described previously in the gravel stratum around the settlements of Vasvár, Sárvár, and Ostffyasszonyfa.^{43,44}

3 | MATERIALS AND METHODS

3.1 | Identification of thermal contraction cracks by remote sensing

Sand wedge polygons have been observed at several locations in the Kemeneshát region, where the post-Pleistocene sediments and soils form a cover (0.6–1 m) over the polygons. The Holocene sediments and the soil horizons visibly differ from the sand wedge infilling but were not examined in this study.

Satellite data from the DigitalGlobe Foundation provide a high-quality dataset with a sub-meter horizontal resolution. Due to their high temporal resolution, it is also possible to find images acquired under favorable weather conditions. The current analysis was based on WorldView-1 panchromatic images of 0.5-m horizontal resolution, acquired on January 8 and 21, 2008. Despite the high spatial resolution, there are patches with low polygon visibility. Therefore, satellite images were simultaneously analyzed in Google Earth Pro™ using the “Historical Imagery” function, since images between 2006 and 2017 were also found to be useful to detect polygonal patterns. Detection was also highly influenced by the varying image quality, unfavorable weather conditions or temporary surface cover (snow or tailing material from the mine).

The applicability of satellite images was checked at two test sites (one by mapping cropmarks, and another one with an excavated surface) by using an unmanned aerial vehicle in the summer of 2019, during a field work campaign. Aerial images were taken with a DJI MAVIC 2 PRO drone, with its Hasselblad L1D-20c camera. The flight altitude of the drone was 50–100 m, depending on the investigated area. Surveying was followed by manual processing of the images, which resulted in orthophotos.

Using GIS data, the topographical and geological characteristics of the delineated forms were also studied.⁴⁵ Based on SRTM-1 (30-m horizontal resolution)⁴⁶ the elevation, slope, and aspect distribution over these polygonal networks were analyzed.

3.2 | Field work

In total, 72 samples from the infilling material of the wedges were collected in the pits of the Szemenye gravel pit mine. The quarry is

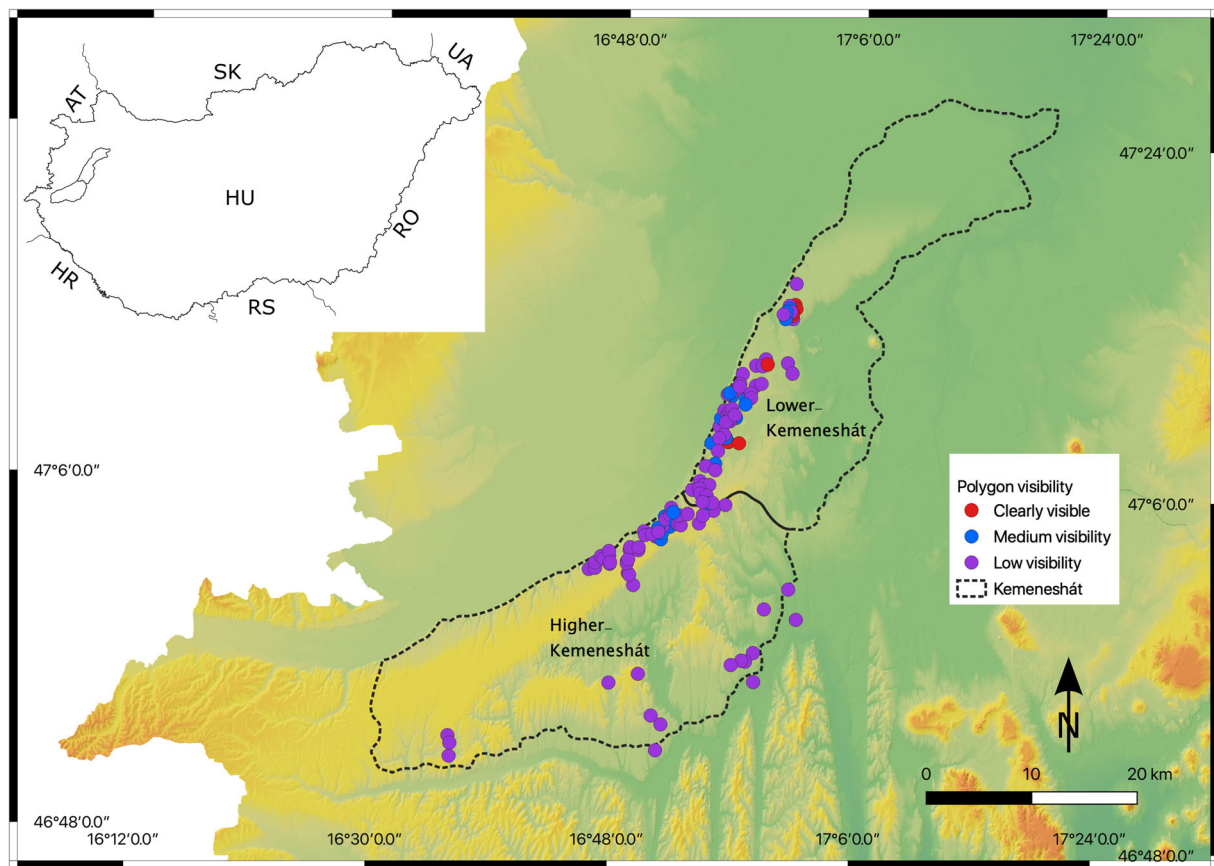


FIGURE 1 Polygon visibility according to satellite imagery (satellite image courtesy of the DigitalGlobe Foundation). Low visibility refers to incomplete polygons, medium visibility refers to polygons where not every part is visible, yet the shapes can be completed, while clearly visible polygons are complete forms.

located at an altitude of ca. 225–230 m a.s.l. Mining activity has ceased in the northern part (also known as the *Csipkerek* site in former publications), while the southern area (Szemenye II) is currently active. Due to the mining activity, Holocene sediments were removed in the southern part of the Szemenye II site, facilitating observation of the polygons. Owing to constant removal of the gravelly host, the identification and description of the vertical profiles were more challenging. Five samples from the cemented host material were also collected to compare their physical properties with the infilling material.

3.3 | Grain size analysis and end-member modeling (EMMA)

The same laboratory performed all sample analyses. After standard drying, the samples were sieved over a 2-mm screen with a Fritsch Analysette Pro 3 shaker. Then, 10 g of each sample was pretreated to remove CaCO_3 and organic matter. The organic matter was removed by hydrogen peroxide (30%, 15–30 ml, depending on the length of the chemical reaction), while carbonates and iron oxide were removed with hydrochloric acid (10%, 15 ml).⁴⁷ After sample preparation, grain

size was determined with a laser diffractometry Malvern Mastersizer 3000 laser diffractometer (Malvern Inc) particle size analyzer.

Raw data were processed in the GRADISTATv8.0 software,⁴⁸ where simple descriptive statistical parameters (e.g., mean, sorting, skewness, and kurtosis) were calculated. In the calculations, the Folk and Ward method was used.⁴⁹ In addition to this calculation, EMMA was also used for further analysis of the sediments.

EMMA is used to unmix sedimentary dynamic populations and was first developed by Weltje.⁵⁰ Since its first use, it has widely been applied in sedimentological analyses.^{51–56} The calculations include the estimation of necessary end-members (EMs; based on the mean total explained variance), the determination of end-member scores and loadings, and the class- and sample-wise explained variance. For this, the EMMAgeo package for R was used.⁵⁷

To obtain a high-quality, reliable model, the possible uncertainties of EMMA^{52,58} were reduced in our case as follows: (a) a standard laser diffraction method was used for grain size measurement; (b) the model parameters were optimized (empty bins were removed from the dataset, the number of samples and grain size bins were more than the lower limit as stated by Dietze et al.⁵⁸); (c) each EM contributes at least 10% by volume of the total loadings; (d) there is no post-depositional mixing in the sand wedge infilling which could lower the

quality of the model (however, according to Dietze et al.⁵⁸ this process has no influence on the EM loadings); and (e) there are no overlapping EMs.

3.4 | Dating the infilling material—OSL

By using OSL it is possible to determine the last time sediment grains were exposed to sunlight; that is, the time of sediment formation or the time of burial of the grains. Where sand was readily available, the OSL ages correspond to the formation of cracks within the error limit of OSL dates.

Sampling was done by hammering steel tubes into the sand wedges (Figure 2). The preparation of samples followed standard laboratory techniques.⁵⁹ All procedures were carried out in subdued yellow light provided by low-pressure sodium lamps. The samples were dried to constant weight to determine in situ water content. Coarse grain sand was separated using sieves of 150- and 220- μm mesh size. The carbonate and organic fractions of samples were removed by repeated acid treatment in 10% HCl and 10% H₂O₂. Extraction of the quartz fraction was done using heavy liquid flotation (LST Fastfloat). Finally, 45 min of etching in 40% HF was performed to remove any remaining feldspar residuals and the outer shell of quartz grains. Quartz extracts were spread on 1-cm stainless steel disks using a 4-mm mask size.

The equivalent dose (D_e) of samples was determined using a RISØ DA-20 TL/OSL-type luminescence reader. Irradiation was made using a calibrated ⁹⁰Sr/⁹⁰Y β -source. OSL was detected with an EMI ET9107-type photomultiplier. Stimulation was carried out using blue LEDs (470 ± 30 nm), while detection was made through a Hoya U-340 filter. Throughout the measurements, the single aliquot regeneration (SAR) protocol was applied.^{60,61} Preheat and dose recovery tests were performed to identify the best measurement parameters and assess the reproducibility of measurements.

Environmental dose rate (D^*) was determined using high-resolution, extended-range gamma-ray spectrometry, applying a Canberra-

type HpGe detector and 450-ml Marinelli beakers. Dry dose rates were calculated using the conversion factors of Liritzis et al.⁶² Wet dose rates were assessed based on in situ water contents.⁶³ The rate of cosmic radiation was determined by considering burial depth, and geographic location, following the equation of Prescott and Hutton.⁶⁴

Since the wedges were only a few decimeters in width, the radioactive element content of both the sand in the wedges and the gravelly host material were measured. Dose rates were weighed according to the volumetric share of the two materials in a 30-cm-diameter sphere around the sample.

4 | RESULTS

4.1 | Polygon morphometry

Over the 1,200-km² study area, 128 sites with possible polygonal networks were delineated from the two DigitalGlobe images. Twenty-eight additional sites were located on Google Earth Pro™ images, which were taken during the vegetative period. The sites were categorized into three visibility categories (clearly visible, medium visibility, and low visibility, Figure 1).

Most features are located at an elevation of 210–230 m a.s.l., which corresponds to the general topography of the Higher Kemencshát microregion along the Rába River. It was also found that the polygonal networks were formed on flat (0–5%) surfaces, mostly facing the N-NW. In terms of surface lithology (i.e., the host material), 50% of the sites are covered by gravel, one-third by loess while the remaining area is overlain by colluvial and fluvial sediments. Satellite imagery revealed that the delineated polygons predominantly have 5–7 sides, the most frequent sizes vary between 13 and 23 m in diameter, whereas the largest polygons reach a diameter of 50–60 m, and the edges intersect at an angle of 110–130° (Figure S1).

Two study sites were mapped with drone imagery, the southern part of the currently active Szemenye gravel pit, and a site with clearly

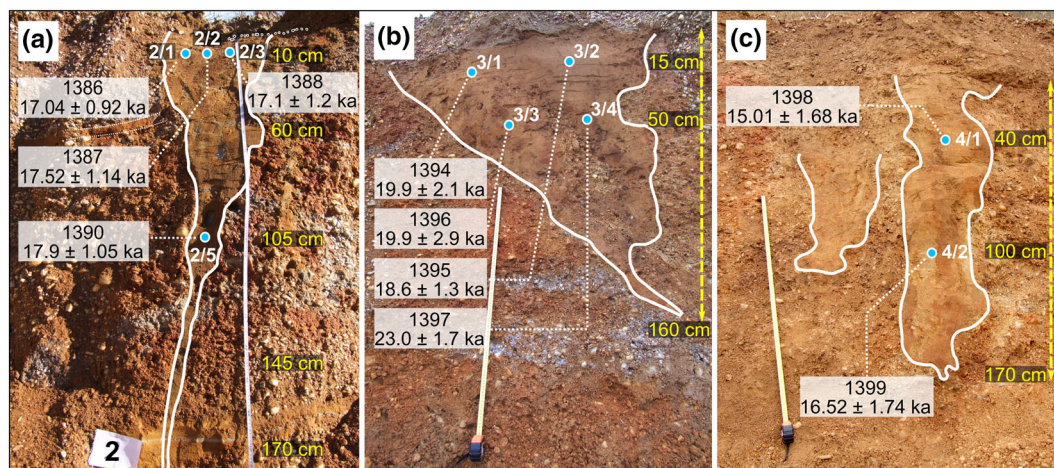


FIGURE 2 Sand wedge excavations with the corresponding OSL ages. A—SZ2 profile, B—SZ3 profile, C—SZ4 profile.

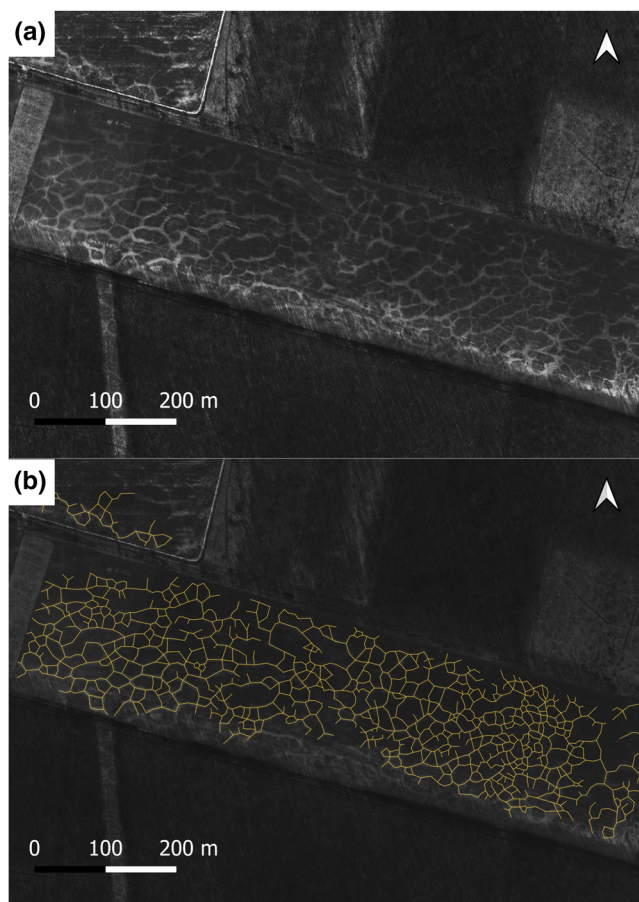


FIGURE 3 Polygonal cropmarks near the village of Bejcgartyános as seen on satellite image in Google Earth Pro™ (a) and its schematic manually interpreted sketch (b).

visible cropmarks near Nyógér. In the pit, the overlying soil was removed during pit exploitation, and the polygonal networks became exposed. At the other site, satellite images showed possible thermal contraction cracks appearing in the cultivated land. Polygons were clearly visible on the aerial drone images (Figure 3).

Due to ongoing mining activities, sampled sand wedges were divided into two main groups, namely “complete” and “incomplete” forms. Whereas the dimensions of “complete” sand wedges are measurable in the field, the approximate sizes of the “incomplete” wedges could only be estimated. There was no visible internal structure in the sampled sand wedges, but grayish microcracks (veins) were observed in some cases where polygons were truncated horizontally during mining operations. These veins, however, were too small for separate sampling. Measured sand wedge depths varied between 1.1 and 2.7 m with widths of 0.45–1.9 m.

4.2 | GSD and EMMA

Twenty-three of the total 72 samples had a unimodal grain size distribution, while the remaining 49 samples had at least two modes

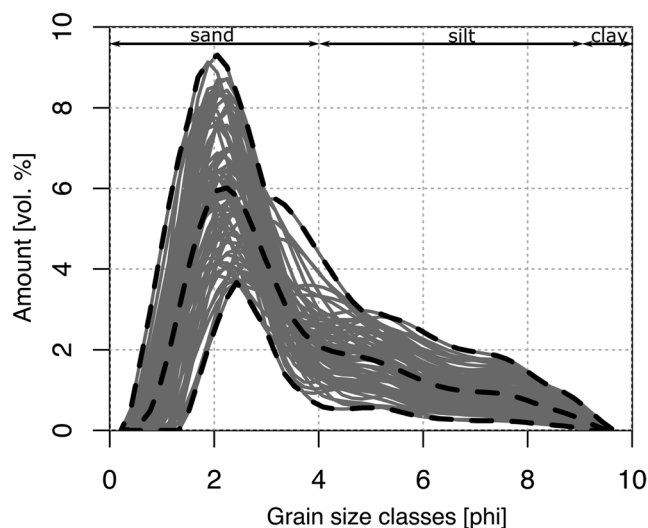


FIGURE 4 Individual grain size distributions of the sand wedge infilling samples ($N = 72$), with the minimum, maximum and mean values highlighted.

(bimodal, trimodal and polymodal samples). All samples are positively skewed and exhibit poor and very poor sorting values (Figure 4, Table S1).

The comparison in Table 1 confirms that the infilling material consists of almost exclusively sand (92.8–96.3%), while the host sediment consists mostly of sandy gravel (49–75% gravel). The clay and silt fraction is also slightly more abundant in the fill (3.5–7%) than in the host sediment (0.8–1.6%).

The EMMA calculations resulted in four different EMs (Figure S2). Their weighting scores are at least 16% (EM1), and at most 39% (EM2) of the total modeled volume. Every EM GSD is polymodal, with two EM modes in the medium sand fraction (EM3 at 1.7 ϕ and EM4 at 1.5 ϕ), one in the fine sand fraction (EM2 at 2.1 ϕ), and one in the very fine sand fraction (EM1 at 3.5 ϕ). Each has additional minor modes, in the sand and silt domains.

The highest EM1 contributions overlap the lowest goodness-of-fit values, whereas samples with the highest EM2 contributions show the highest R^2 values. Eighteen samples contain all EMs, while there are at least two EMs in each sample except sample (field ID: SZ6_4; lab code: 57). Samples with the highest EM2 contributions have very low EM3 volumes, while the highest EM1 values are associated with the lowest EM2 and EM4 percentages.

4.3 | Luminescence characteristics and ages

For samples OSZ 1386 (SZ 2/1 profile) and OSZ 1390 (SZ 2/5 profile), a combined preheat and dose recovery test was performed. In the tests, we investigated the optimal temperature at which the luminescence properties of the sample are the most stable. The parameters considered were: recycling ratio and dose recovery ratio should ideally be close to 1, while recuperation should be below 5%, and each

TABLE 1 Comparison of fractions of the host sediment and the infilling material of the wedges. Grain size classes were determined according to Blott and Pye.⁶⁵

Field ID (lab code)	Host sediment			Infilling material		
	Silt and clay (%)	Sand (%)	Gravel ^a (%)	Silt and clay (%)	Sand (%)	Gravel (%)
SZ1 (66)	1.6	23.4	75	3.5	95.8	0.7
SZ2 (67)	1.0	30.2	68.8	5.2	94.7	0.1
SZ3 (68)	0.8	38.3	60.9	3.5	96.3	0.2
SZ6_1 (1)	1.1	50.0	48.9	6	93.9	0.1
SZ6_2 (2)	1.0	28.8	70.2	7	92.8	0.2

^aGravels and boulders >16 mm were removed from the samples before sieving to avoid distorted results. In this case, infilling samples were sieved for comparable results, and therefore the data are in mass percentage.

parameter should have a maximum error of 10%.⁶¹ Those aliquots that did not pass the criteria listed above were rejected and not used for further calculations.

The measurements show that the recycling and dose recovery ratios for most samples had a large uncertainty at each preheat temperature (Figure S3). For example, for sample OSZ 1390, the recycling ratio was below 1.1 only at 220°C. The results are closest to the ideal usually set at 220°C and the accuracy of results was also best at this temperature (Figure S4). Thus, preheat temperature was set to this value during the SAR measurements.

SAR measurements generated a low intensity (i.e., the samples were relatively insensitive), which made the evaluation difficult. Thus, more than three-quarters of the aliquots of the measured samples did not meet the SAR criteria and had to be rejected.

Note that some aliquots that produced low signal intensities also showed lower equivalent doses. However, because the results of these samples did not meet the evaluation criteria, they did not affect the calculation of the equivalent dose for the sample.

Samples were evaluated following the recommendations of Arnold et al.⁶⁶ Thus, we examined the accepted results for skewness, kurtosis, and overdispersion. For samples where the overdispersion value exceeded 30%, the Minimum Age Model (MAM) was used, while in the other cases the Central Age Model (CAM) model was applied (Table S2).

5 | DISCUSSION

5.1 | Sand wedge polygon morphometry and its relation to the geological and geomorphological conditions

Our findings are in agreement with the literature on relict polygonal patterned ground structures. The values obtained show a strong similarity in size (width of the wedges and diameter of the polygons) and appearance (geometry) with the forms found in other regions of Europe.^{9,21,67,68} Based on these characteristics, from the categories of Ewertowski et al.,⁹ irregular, small, nonorthogonal polygons are most common over the Kemeneshát region. A recent comprehensive

analysis on thermal contraction crack polygons in Europe by Bertran⁶⁹ strengthens our results, with additional data on the role of topography. Bertran⁶⁹ states that nonorthogonal, hexagonal polygons usually appear on well-drained reliefs, such as the NW edge of the Kemeneshát area, where most of the polygons were identified. However, the inner parts of the region have lower slope gradients and poor drainage, which is less ideal for the cited forms. The diameter values are also consistent with the dimensions of thermal contraction crack polygons described in recent arctic regions.⁷⁰

The broad occurrence of the well-preserved polygonal networks is due to the morphological and geological settings of the former Rába alluvial plain. However, cropmarks were visible only during favorable conditions, which suggests that the actual number of polygons is probably larger. Analysis on a large dataset by Bertran⁶⁹ reinforces this assumption.

Based on our observations, we suggest the use of satellite images for bulk datasets owing to the smaller file size and ease of processing, while drone imagery can be a useful tool for individual study sites for more detailed analysis.

5.2 | Characteristics of the infilling

Poor and very poor sorting values suggest that the transportation process of the material did not last long. According to the summary of Murton et al.,¹⁴ this seemingly heterogenic infill is uncommon, but not absent for sand wedges. The inconsistency among particle size distributions attests to the complex origin of the infilling material, and the mean sand:silt:clay ratio of 67:32:1 reinforces this uncertainty. As stated previously, the strongly cemented host material is very different from the sandy infilling. In contrast to the observations described by many authors (e.g., Black,⁷¹ Murton and Bateman⁷²) the examined wedges lack vertical lamination. This was probably due to the melting of ice veins or secondary perturbation. The polymodal distributions of EM loadings, along with the GSDs point to brief wind activity. The grain size distribution suggests that the material was mainly transported by rolling and saltation (coarser fractions), while modified saltation and short-term suspension also played an important role in the process of filling of the frost cracks

(cf. figure 1 in Tsoar and Pye⁷³). There is also a notable amount that was probably transported in long-term suspension (silt and clay fractions), although their source has not yet been identified. However, the infill may originate from a mixture of eolian sand and material provided by the collapse of the surrounding host material (in the present case gravel). When eolian sand is unavailable, the collapse of host sediment is the only process involved in the filling of the crack.^{74,75} In addition, the fine-grained fraction may derive from washing of the host sediments, so there is no clear evidence of an allochthonous origin of this fraction.

5.3 | Absolute ages and regional correlations

The OSL age estimates reliably date the time of wedge development rather than post-depositional wedge modifications.³³ Our measurements point to an MIS 2 Greenland Stadial (GS)-2.1a–c origin for the sand wedges, which fits well with the general concept of the periglacial domain in Europe. Andrieux et al,²² based on 86 age estimates from single grain OSL dating of 33 samples from relict sand and composite wedge infillings, identified 11 sand wedge activity phases in France over the last 100 ka. Phases 3–6 (from 15.3 ± 0.4 to 24 ± 1.1 ka) overlap the results with the Hungarian OSL ages (Fábíán et al²⁸ and this study, Figure 5), as well as with Polish⁹ and Belgian³⁰ numerical ages.

Since OSL ages were determined on aliquots each comprising multiple grains potentially belonging to different phases of wedge filling, the estimates obtained here should be considered indicative of the main periods during which the filling was formed.

Strong wind activity was reportedly present in the Pannonian Basin during the Pleistocene, as testified by mega-yardangs⁴¹ and ventifacts.⁴⁰

5.4 | The interpretation of paleoclimatic proxies in the Pannonian Basin—limitations and possibilities

There are several proxies which have been used to reconstruct paleoclimatic conditions during the LGM in the Pannonian Basin, such as data retrieved from groundwater recharge temperature,⁷⁸ pollen analysis,⁷⁹ and malacological data,^{80–83} and stable isotope signal of mammoth tusk dentin⁸⁴ findings. Certain problems arose, however, when trying to put the results together; namely, their spatial distribution is rather sporadic, and they point to different climatic parameters, that is determining the mean annual air temperature (MAAT) or the mean temperature of the warmest month (MTWA). It is also challenging to compare field evidence with global or regional climate model simulations, because the models do not include proxies from all modeled areas (e.g., the model by Strandberg et al⁸⁵ has no proxies for the Pannonian Basin).

For example, data extracted by the malaco-thermometer method of Sümegi et al⁸¹ from land snail assemblages point to ca. 12–17°C MTWA during MIS 2, fluctuating in good correspondence with the changes in the oxygen isotope data.^{81,82} The same method was used to obtain information on July paleotemperatures in southern Hungary and northern Serbia, with the conclusion of increasing values southward (MTWA changed from $15.1 \pm 2.3^\circ\text{C}$ at the Madaras loess section to 19.6 ± 1.2 at the Pozarevac study site) during the LGM.⁸³

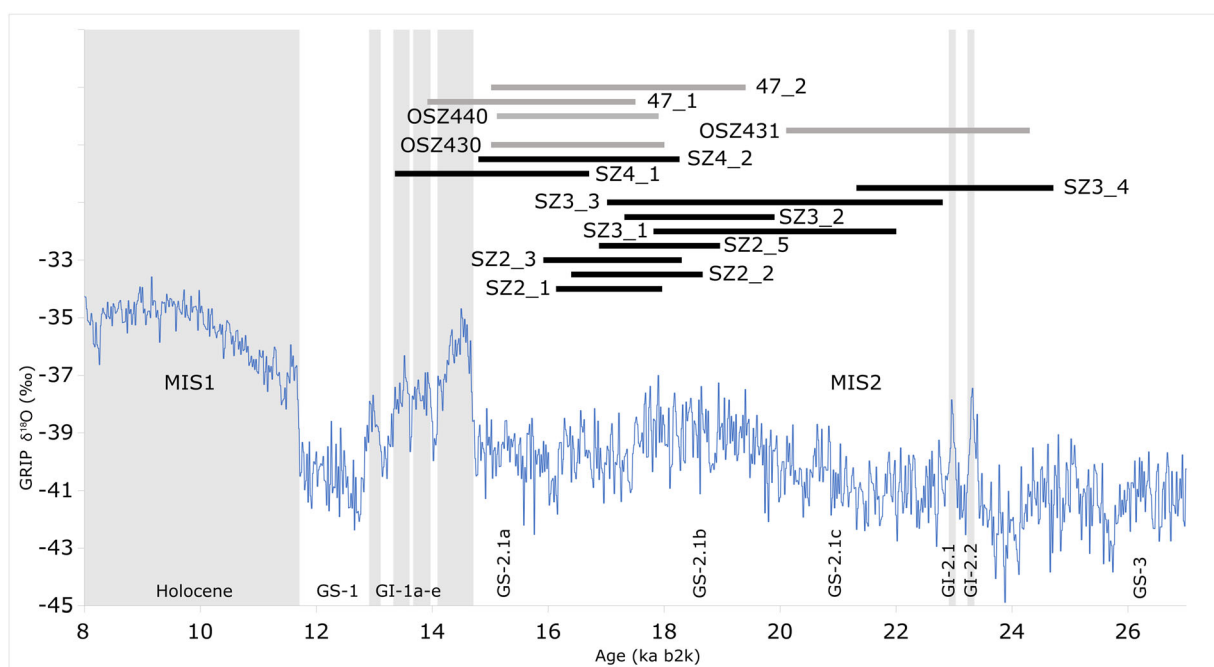


FIGURE 5 OSL chronology of the sand wedges of the Pannonian Basin, Hungary, against the isotope record from Seierstad et al⁷⁶ and stratigraphic record from Rasmussen et al.⁷⁷ Gray: Fábíán et al,²⁸ black: this study.

Although these temperatures may seem too high for frost-related processes as proposed by Kovács et al.,²⁹ there is currently a July mean temperature of 17°C through territories with discontinuous/sporadic permafrost or deep seasonal frost in the subarctic Canada where thermal contraction cracks (sand wedges) have been identified.⁷ Very similar MTWA values are also reported in Siberia today in permafrost-affected terrain (ncei.noaa.gov in Zepner⁸⁶). Palynological data revealed a mosaic of mixed forest–steppe structure (birch, alder, willow, Norway pine) with patches of taiga and cold steppe, but also scattered tundra-like vegetation, while malacological studies identified cold-loving, then cold-tolerant terrestrial snail fauna in the basin throughout the LGM.^{79,82,87} $\delta^{18}\text{O}$ data derived from mammoth tusk dentin samples suggest an MAAT of 2.4°C for 21.250 ± 0.45 ka cal BP (village of Zók) and 8.1°C for 16.249 ± 0.413 ka cal BP (village of Csajág).⁸⁴ According to Fricke and O'Neil,⁸⁸ however, the present-day oxygen isotope ratio and temperature relationship is not an entirely reliable source to infer “ice age” surface air temperatures.

There is another, quantitative, terrestrial, low-elevation paleotemperature proxy which has been used in the Pannonian Basin for LGM climate reconstruction, the so-called noble gas temperature (NGT) method.⁷⁸ This method is based on the temperature-dependent solubility of noble gases during groundwater recharge and is often associated with groundwater ^{14}C dating to pair numerical ages to temperatures.^{89,90} Varsányi et al.⁷⁸ dated and measured 16 samples from the south-eastern part of Hungary to reconstruct paleoclimatic conditions for the LGM to Holocene. The study found that from 24.488 to 14.683 ka cal BP, NGT values ranged from 4.65 ± 0.53 to 11.57 ± 0.57°C (cf. table 4 in Varsányi et al.⁷⁸; only values with at least 60% probability were considered from that article). Noble gas temperature, however, is an indicator of long-term water table temperature (WTT), not of surface air temperature (SAT), as emphasized by Cey.⁹¹ Cey⁹¹ also suggests that snow cover changes caused by glacial–interglacial atmospheric temperature change result in an underestimation of that atmospheric temperature change as inferred from dissolved noble gas data. Temperatures >4°C suggest that the sampled area (the southern part of the Great Hungarian Plain) was not under permafrost during the LGM. However, the possibility that the coldest phases of the LGM were not captured by the analyses of aquifer NGTs should be kept in mind.

The LGM permafrost simulation by Stadelmaier et al.⁹² failed to reconstruct permafrost in the study area at a depth of −0.7 m. By contrast, Bertran et al.,⁹³ using the same climate model but considering a representative ground level of −1.5 m, were able to reconstruct discontinuous permafrost in Hungary. Active layer thickness (ALT) was found to have ranged between 2 and 3 m in the region. Together, this suggests strongly that (a) the area was close to the southern permafrost boundary and (b) the sand wedges developed within the active layer or in a context of deep seasonal frost (depending on local parameters). The sand wedges have an average depth of 2–3 m, which is around the same as the probable ALT. This also suggests strongly that the lack of vertical lamination in the wedges is not due to the melting of ice veins but more probably to secondary perturbation.

After considering European past permafrost-related field evidence, we cannot exclude the possibility of a spatially and temporally fluctuating environment in the Pannonian Basin, thus varying from permafrost to deep seasonal frost. Based on our findings, we can say that among the several, already identified cooling periods (i.e., the possibility of permafrost), the Pannonian Basin may have only been affected by the last one (MIS 2 GS 2.1a–c), since no older OSL ages have yet been found in the region. We must keep in mind that conventional OSL dating of sand wedges does not allow the identification of distinct phases of sand filling, but provides only an estimate of the main period of filling. However, distinguishing the exact paleoenvironmental conditions cannot be made with certainty.

6 | CONCLUSIONS

Sand-filled thermal contraction cracks are more common relict landforms in the western part of Hungary than elsewhere in the country. Within the study area, the polygons generally appear at 210–230 m a.s.l., mostly in gravel and loess. The infilling material for the wedge-shaped forms is poorly sorted fine sand. The youngest OSL date indicates that eolian activity may have taken place as late as 15.01 ± 1.68 ka BP and such material was able to fill the cracks. As far as the sand filling was synchronous or just slightly delayed compared to crack formation, we assume that climatic conditions during the dated periods were cold enough in winter to generate patterns of soil thermal contraction cracks at the study site. Our research has shown that high-resolution satellite imagery is applicable for the mapping of large polygon networks, while drone photos are more suitable for detailed analysis over a single study site of thermal contraction crack polygons. OSL dating was a useful tool for determining the timing of such geomorphological processes, and based on the compared data (from France), three or four phases of wedge formation are presumed. Although our data did not ascertain the exact period of frost-related activity in the Pannonian Basin, the geomorphological, sedimentological and absolute dating evidence indicate that cold and dry climate episodes in MIS GS 2 shaped the landscape in the Pannonian Basin.

ACKNOWLEDGEMENTS

DigitalGlobe Foundation is gratefully acknowledged for the satellite images. The authors are also grateful for Professor Barbara Woronko (University of Warsaw) for useful comments that improved the quality of the manuscript. The authors thank reviewers Pascal Bertran and Michel Allard, as well as editor in chief Professor Mauro Guglielmin for their valuable comments and remarks that significantly contributed to the paper.

DATA AVAILABILITY STATEMENT

The data that support the findings of this study are available from the corresponding author upon reasonable request.

ORCID

Beáta Farkas  <https://orcid.org/0000-0002-7026-8980>

REFERENCES

1. French HM. *The periglacial environment*. John Wiley & Sons, Ltd; 2007. doi:10.1002/9781118684931
2. Buol SW, Southard RJ, Graham RC, McDaniel PA. *Soil genesis and classification*. Wiley; 2011. doi:10.1002/9780470960622
3. Li JH, Zhang LM. Study of desiccation crack initiation and development at ground surface. *Eng Geol*. 2011;123(4):347-358. doi:10.1016/j.enggeo.2011.09.015
4. Lachenbruch AH. Mechanics of thermal contraction cracks and ice-wedge polygons in permafrost. In: *SIAM Monographs on Mathematical Modeling and Computation*; 1962:1-66. doi:10.1130/SPE70-p1
5. Lachenbruch AH. Contraction theory of ice-wedge polygons; a qualitative discussion. In: *First international permafrost conference*. National Academy of Science, National Research Council of Canada; 1966: 63-71.
6. Watanabe T, Matsuoka N, Christiansen HH. Ice- and soil-wedge dynamics in the Kapp Linné area, Svalbard, investigated by two- and three-dimensional GPR and ground thermal and acceleration regimes. *Permafrost Periglacial Process*. 2013;24(1):39-55. doi:10.1002/ppp.1767
7. Wolfe SA, Morse PD, Neudorf CM, Kokelj SV, Lian OB, O'Neill HB. Contemporary sand wedge development in seasonally frozen ground and paleoenvironmental implications. *Geomorphology*. 2018;308:215-229. doi:10.1016/j.geomorph.2018.02.015
8. Rodríguez-López JP, Wu C, Vishnivetskaya TA, Murton JB, Tang W, Ma C. Permafrost in the cretaceous supergreenhouse. *Nat Commun*. 2022;13(1):7946. doi:10.1038/s41467-022-35676-6
9. Ewertowski MW, Kijowski A, Szuman I, Tomczyk AM, Kasprzak L. Low-altitude remote sensing and GIS-based analysis of cropmarks: classification of past thermal-contraction-crack polygons in central western Poland. *Geomorphology*. 2017;293:418-432. doi:10.1016/j.geomorph.2016.07.022
10. Christiansen HH, Matsuoka N, Watanabe T. Progress in understanding the dynamics, internal structure and Palaeoenvironmental potential of ice wedges and sand wedges. *Permafrost Periglacial Process*. 2016; 27(4):365-376. doi:10.1002/ppp.1920
11. Bockheim J, Coronato A, Rabassa J, Ercolano B, Ponce J. Relict sand wedges in southern Patagonia and their stratigraphic and paleoenvironmental significance. *Quat Sci Rev*. 2009;28(13-14):1188-1199. doi:10.1016/j.quascirev.2008.12.011
12. Kasse C, Vandenberghe J. Topographic and drainage control on Weichselian ice-wedge and sand-wedge formation, Vennebrügge, German-Dutch border. *Permafrost Periglacial Process*. 1998;9(2):95-106. doi:10.1002/(SICI)1099-1530(199804/06)9:2%3C95::AID-PPP282%3E3.0.CO;2-D
13. Rémillard AM, Héту B, Bernatchez P, et al. Chronology and palaeoenvironmental implications of the ice-wedge pseudomorphs and composite-wedge casts on the Magdalen Islands (eastern Canada). *Boreas*. 2015;44(4):658-675. doi:10.1111/bor.12125
14. Murton JB, Worsley P, Gozdzik J. Sand veins and wedges in cold aeolian environments. *Quat Sci Rev*. 2000;19(9):899-922. doi:10.1016/S0277-3791(99)00045-1
15. Vandenberghe J, French HM, Gorbunov A, et al. The last permafrost maximum (LPM) map of the northern hemisphere: permafrost extent and mean annual air temperatures, 25-17 ka BP. *Boreas*. 2014;43(3): 652-666. doi:10.1111/bor.12070
16. Poser H. Boden- und Klimaverhältnisse in Mittel- und Westeuropa während der Würmeiszeit. *Erdkunde*. 1948;2(1):53-68. doi:10.3112/erdkunde.1948.01.03
17. Kaiser K. Klimazeugen des periglazialen Dauerfrostbodens in Mittel- und West-Europa. *Eiszeitalt Ggw*. 1960;11:121-141.
18. Maarleveld GC. *Periglacial phenomena and the mean annual temperature during the last glacial time in the Netherlands*. Biul PeryglacPublished online; 1976.
19. Velichko A. In: Gerassimov IP, ed. *Paleogeography of Europe during the last one hundred thousand years*. Nauka; 1982.
20. Ruzkiczay-Rüdiger Z, Kern Z. Permafrost or seasonal frost? A review of paleoclimate proxies of the last glacial cycle in the east central European lowlands. *Quat Int*. 2016;415:241-252. doi:10.1016/j.quaint.2015.07.027
21. Andrieux E, Bertran P, Saito K. Spatial analysis of the French Pleistocene permafrost by a GIS database. *Permafrost Periglacial Process*. 2016; 27(1):17-30. doi:10.1002/ppp.1856
22. Andrieux E, Bateman MD, Bertran P. The chronology of Late Pleistocene thermal contraction cracking derived from sand wedge OSL dating in central and southern France. *Global Planet Change*. 2018;162: 84-100. doi:10.1016/j.gloplacha.2018.01.012
23. Szádecky-Kardoss E. Pleistozäne Strukturbodenbildung in den ungarischen Tiefebene und im Wiener Becken. *Földt Közlöny*. 1936;22: 213-228.
24. Kerekes J. *Fosszilis tundraalaj a Bükkben*. Földrajzi KözleményekPublished Online; 1938:112-116.
25. Kerekes J. *A pestszentlőrinci fosszilis tundraképződmények*. Földt KözlönyPublished Online; 1939:131-139.
26. Kerekes J. *Hazánk periglaciális képződményei*. Beszám Magy Királyi Földt Intéz Vitaüléseinek MunkálatairóPublished online; 1941.
27. Pécsi M. Chronological problem of the patterned soils of Hungary. *Biul Peryglac*. 1964;14:279-293.
28. Fábán SÁ, Kovács J, Varga G, et al. Distribution of relict permafrost features in the Pannonian Basin, Hungary. *Boreas*. 2014;43(3):722-732. doi:10.1111/bor.12046
29. Kovács J, Fábán SÁ, Schweitzer F, Varga G. A relict sand-wedge polygon site in north-Central Hungary. *Permafrost Periglacial Process*. 2007; 18(4):379-384. doi:10.1002/ppp.600
30. Buylaert JPP, Ghysels G, Murray AS, et al. Optical dating of relict sand wedges and composite-wedge pseudomorphs in Flanders, Belgium. *Boreas*. 2009;38(1):160-175. doi:10.1111/j.1502-3885.2008.00037.x
31. Bateman MD. Luminescence dating of periglacial sediments and structures. *Boreas*. 2008;37(4):574-588. doi:10.1111/j.1502-3885.2008.00050.x
32. Böse M. Gravel analysis of Weichselian tills and OSL dates of sand wedges in western Poland. *Quaest Geogr*. 2000;21(September): 39-45.
33. Guhl A, Bertran P, Zielhofer C, Fitzsimmons KE. Optically stimulated luminescence (OSL) dating of sand-filled wedge structures and their fine-grained host sediment from Jonzac, SW France. *Boreas*. 2013; 42(2):317-332. doi:10.1111/j.1502-3885.2012.00270.x
34. Liu XJ, Lai ZP. Optical dating of sand wedges and ice-wedge casts from Qinghai Lake area on the northeastern Qinghai-Tibetan plateau and its palaeoenvironmental implications. *Boreas*. 2013;42(2):333-341. doi:10.1111/j.1502-3885.2012.00288.x
35. Schaetzl RJ, Running G, Larson P, Rittenour T, Yansa C, Faulkner D. Luminescence dating of sand wedges constrains the late Wisconsin (MIS 2) permafrost interval in the upper Midwest, USA. *Boreas*. 2021; 51(2):385-401. doi:10.1111/bor.12550
36. Nissen TC, Mears B. Late pleistocene ice-wedge casts and sand-wedge relics in the Wyoming basins, USA. *Permafrost Periglacial Process*. 1990;1(3-4):201-219. doi:10.1002/ppp.3430010302
37. Wayne WJ. Ice-wedge casts of Wisconsinian age in eastern Nebraska. *Permafrost Periglacial Process*. 1991;2(3):211-223. doi:10.1002/ppp.3430020305
38. Fisher TG. Sand-wedge and ventifact palaeoenvironmental indicators in north-West Saskatchewan, Canada, 11 ka to 9.9 ka BP. *Permafrost Periglacial Process*. 1996;7(4):391-408. doi:10.1002/(SICI)1099-1530(199610)7:4%3C391::AID-PPP229%3E3.0.CO;2-W
39. Ribolini A, Bini M, Consoloni I, et al. Late-pleistocene wedge structures along the patagonian coast (argentina): chronological constraints and palaeo-environmental implications. *Geogr Ann Ser Phys Geogr*. 2014;96(2):161-176. doi:10.1111/geoa.12038
40. Jámor Á. A magyarországi pleisztocén éleskavics előfordulások és földtani jelentőségük. *Földt Közlöny*. 2002;132(különszám):101-116.

41. Sebe K, Csillag G, Ruzsiczay-Rüdiger Z, et al. Wind erosion under cold climate: a Pleistocene periglacial mega-yardang system in Central Europe (Western Pannonian Basin, Hungary). *Geomorphology*. 2011; 134(3-4):470-482. doi:[10.1016/j.geomorph.2011.08.003](https://doi.org/10.1016/j.geomorph.2011.08.003)
42. Clark PU, Dyke AS, Shakun JD, et al. The last glacial maximum. *Science*. 2009;325(5941):710-714. doi:[10.1126/science.1172873](https://doi.org/10.1126/science.1172873)
43. Somogyi S. A Vasi-Hegyhat és a Kemeneshát. *Földrajzi Ért.* 1962; 11(1):52-57.
44. Ádám L. A Rábántúli kavicsstakaró. *Földrajzi Ért.* 1962;11(1):41-51.
45. Gyalog L, Síkhegyi F. *Magyarország Földtani Térképe M=1:100 000*. Magyar Állami Földtani Intézet; 2005.
46. Earth Resources Observation And Science (EROS) Center. *Shuttle radar topography Mission (SRTM) 1 arc-second global*. Published Online; 2017. doi:[10.5066/F7PR7TFT](https://doi.org/10.5066/F7PR7TFT)
47. Konert M, Vandenberghe J. Comparison of laser grain size analysis with pipette and sieve analysis: a solution for the underestimation of the clay fraction. *Sedimentology*. 1997;44(3):523-535. doi:[10.1046/j.1365-3091.1997.d01-38.x](https://doi.org/10.1046/j.1365-3091.1997.d01-38.x)
48. Blott SJ, Pye K. GRADISTAT: a grain size distribution and statistics package for the analysis of unconsolidated sediments. *Earth Surf Process Landf.* 2001;26(11):1237-1248. doi:[10.1002/esp.261](https://doi.org/10.1002/esp.261)
49. Folk RL, Ward WC. Brazos River bar [Texas]; a study in the significance of grain size parameters. *J Sediment Res.* 1957;27(1):3-26.
50. Weltje GJ. End-member modeling of compositional data: numerical-statistical algorithms for solving the explicit mixing problem. *Math Geol.* 1997;29(4):503-549. doi:[10.1007/BF02775085](https://doi.org/10.1007/BF02775085)
51. Dietze E, Hartmann K, Diekmann B, et al. An end-member algorithm for deciphering modern detrital processes from Lake sediments of lake Donggi Cona, NE Tibetan plateau, China. *Sediment Geol.* 2012; 243-244:169-180. doi:[10.1016/j.sedgeo.2011.09.014](https://doi.org/10.1016/j.sedgeo.2011.09.014)
52. Dietze E, Maussion F, Ahlborn M, et al. Sediment transport processes across the Tibetan plateau inferred from robust grain-size end members in lake sediments. *Clim Past.* 2014;10(1):91-106. doi:[10.5194/cp-10-91-2014](https://doi.org/10.5194/cp-10-91-2014)
53. Toonen WHJ, Winkels TG, Cohen KM, Prins MA, Middelkoop H. Lower Rhine historical flood magnitudes of the last 450 years reproduced from grain-size measurements of flood deposits using end member modelling. *Catena*. 2015;130:69-81. doi:[10.1016/j.catena.2014.12.004](https://doi.org/10.1016/j.catena.2014.12.004)
54. Prins MA, Vriend M. Glacial and interglacial eolian dust dispersal patterns across the Chinese loess plateau inferred from decomposed loess grain-size records. *Geochim Geophys Geosyst.* 2007;8(7):1-17. doi:[10.1029/2006GC001563](https://doi.org/10.1029/2006GC001563)
55. Jiang Q, Hao Q, Peng S, Qiao Y. Grain-size evidence for the transport pathway of the Xiashu loess in northern subtropical China and its linkage with fluvial systems. *Aeolian Res.* 2020;46(August):100613. doi:[10.1016/j.aeolia.2020.100613](https://doi.org/10.1016/j.aeolia.2020.100613)
56. Varga G, Újvári G, Kovács J. Interpretation of sedimentary (sub)populations extracted from grain size distributions of central European loess-paleosol series. *Quat Int.* 2019;502:60-70. doi:[10.1016/j.quaint.2017.09.021](https://doi.org/10.1016/j.quaint.2017.09.021)
57. Dietze E, Dietze M. Grain-size distribution unmixing using the R package EMMAgeo. *E&G Quat Sci J.* 2019;68(1):29-46. doi:[10.5194/egqsj-68-29-2019](https://doi.org/10.5194/egqsj-68-29-2019)
58. Dietze M, Schulte P, Dietze E. Application of end-member modelling to grain-size data: constraints and limitations. *Sedimentology* Published Online August. 2021;69(2):845-863. doi:[10.1111/sed.12929](https://doi.org/10.1111/sed.12929)
59. Mauz B, Bode T, Mainz E, et al. The luminescence dating laboratory at the University of Bonn: equipment and procedures. *Anc TL.* 2002; 20(2):53-61.
60. Murray AS, Wintle AG. Luminescence dating of quartz using an improved single-aliquot regenerative-dose protocol. *Radiat Meas.* 2000;32(1):57-73. doi:[10.1016/S1350-4487\(99\)00253-X](https://doi.org/10.1016/S1350-4487(99)00253-X)
61. Wintle AG, Murray AS. A review of quartz optically stimulated luminescence characteristics and their relevance in single-aliquot regeneration dating protocols. *Radiat Meas.* 2006;41(4):369-391. doi:[10.1016/j.radmeas.2005.11.001](https://doi.org/10.1016/j.radmeas.2005.11.001)
62. Liritzis I, Stamoulis K, Papachristodoulou C, Ioannides K. A re-evaluation of radiation dose-rate conversion factors. *Mediterr Archaeol Archaeom.* 2013;13(3):1-15.
63. Aitken MJ. *Thermoluminescence dating*. Academic Press; 1985.
64. Prescott JR, Hutton JT. Cosmic ray contributions to dose rates for luminescence and ESR dating: large depths and long-term time variations. *Radiat Meas.* 1994;23(2-3):497-500. doi:[10.1016/1350-4487\(94\)90086-8](https://doi.org/10.1016/1350-4487(94)90086-8)
65. Blott SJ, Pye K. Particle size scales and classification of sediment types based on particle size distributions: review and recommended procedures. *Sedimentology.* 2012;59(7):2071-2096. doi:[10.1111/j.1365-3091.2012.01335.x](https://doi.org/10.1111/j.1365-3091.2012.01335.x)
66. Arnold LJ, Bailey RM, Tucker GE. Statistical treatment of fluvial dose distributions from southern Colorado arroyo deposits. *Quat Geochronol.* 2007;2(1-4):162-167. doi:[10.1016/j.quageo.2006.05.003](https://doi.org/10.1016/j.quageo.2006.05.003)
67. Bertran P, Andrieux E, Antoine P, et al. Distribution and chronology of Pleistocene permafrost features in France: database and first results. *Boreas.* 2014;43(3):699-711. doi:[10.1111/bor.12025](https://doi.org/10.1111/bor.12025)
68. Ghysels G, Heyse I. Composite-wedge pseudomorphs in Flanders, Belgium. *Permafrost Periglacial Process.* 2006;17(2):145-161. doi:[10.1002/ppp.552](https://doi.org/10.1002/ppp.552)
69. Bertran P. Distribution and characteristics of Pleistocene ground thermal contraction polygons in Europe from satellite images. *Permafrost Periglacial Process.* 2022;33(December 2021):1-15. doi:[10.1002/ppp.2137](https://doi.org/10.1002/ppp.2137)
70. French HM, Demitroff M. Cold-climate origin of the enclosed depressions and wetlands ('spungs') of the pine barrens, southern New Jersey, USA. *Permafrost Periglacial Process.* 2001;12(4):337-350. doi:[10.1002/ppp.401](https://doi.org/10.1002/ppp.401)
71. Black RF. Periglacial features indicative of permafrost: ice and soil wedges. *Quatern Res.* 1976;6(1):3-26. doi:[10.1016/0033-5894\(76\)90037-5](https://doi.org/10.1016/0033-5894(76)90037-5)
72. Murton JB, Bateman MD. Syngenetic sand veins and anti-syngenetic sand wedges, Tuktoyaktuk coastlands, western Arctic Canada. *Permafrost Periglacial Process.* 2007;18(1):33-47. doi:[10.1002/ppp.577](https://doi.org/10.1002/ppp.577)
73. Tsoar H, Pye K. Dust transport and the question of desert loess formation. *Sedimentology.* 1987;34(1):139-153. doi:[10.1111/j.1365-3091.1987.tb00566.x](https://doi.org/10.1111/j.1365-3091.1987.tb00566.x)
74. Friedman JD, Johansson CE, Oskarsson N, Svensson H, Thorarinnsson S, Williams RS. Observations on Icelandic polygon surfaces and Palsa areas. *Photo Interpretation and Field Studies. Geogr Ann Ser Phys Geogr.* 1971;53(3-4):115-145. doi:[10.1080/04353676.1971.11879841](https://doi.org/10.1080/04353676.1971.11879841)
75. Jetchick E, Allard M. Soil wedge polygons in northern Québec: description and paleoclimatic significance. *Boreas.* 2008;19(4):353-365. doi:[10.1111/j.1502-3885.1990.tb00140.x](https://doi.org/10.1111/j.1502-3885.1990.tb00140.x)
76. Seierstad IK, Abbott PM, Bigler M, et al. Consistently dated records from the Greenland GRIP, GISP2 and NGRIP ice cores for the past 104 ka reveal regional millennial-scale $\delta^{18}O$ gradients with possible Heinrich event imprint. *Quat Sci Rev.* 2014;106:29-46. doi:[10.1016/j.quascirev.2014.10.032](https://doi.org/10.1016/j.quascirev.2014.10.032)
77. Rasmussen SO, Bigler M, Blockley SP, et al. A stratigraphic framework for abrupt climatic changes during the last glacial period based on three synchronized Greenland ice-core records: refining and extending the INTIMATE event stratigraphy. *Quat Sci Rev.* 2014;106:14-28. doi:[10.1016/j.quascirev.2014.09.007](https://doi.org/10.1016/j.quascirev.2014.09.007)
78. Varsányi I, Palcsu L, Kovács LÓ. Groundwater flow system as an archive of palaeotemperature: Noble gas, radiocarbon, stable isotope and geochemical study in the Pannonian Basin, Hungary. *Appl Geochem.* 2011;26(1):91-104. doi:[10.1016/j.apgeochem.2010.11.006](https://doi.org/10.1016/j.apgeochem.2010.11.006)
79. Magyari EK, Kuneš P, Jakab G, et al. Late Pleniglacial vegetation in eastern-Central Europe: are there modern analogues in Siberia? *Quat Sci Rev.* 2014;95:60-79. doi:[10.1016/j.quascirev.2014.04.020](https://doi.org/10.1016/j.quascirev.2014.04.020)

80. Sümegi P, Krolopp E. Quaternary malacological analyses for modeling of the upper Weichselian palaeoenvironmental changes in the Carpathian Basin. *Quat Int.* 2002;91(1):53-63. doi:[10.1016/S1040-6182\(01\)00102-1](https://doi.org/10.1016/S1040-6182(01)00102-1)
81. Sümegi P, Molnár D, Gulyás S, et al. High-resolution proxy record of the environmental response to climatic variations during transition MIS3/MIS2 and MIS2 in Central Europe: the loess-paleosol sequence of Katymár brickyard (Hungary). *Quat Int.* 2019;504(March 2018):40-55. doi:[10.1016/j.quaint.2018.03.030](https://doi.org/10.1016/j.quaint.2018.03.030)
82. Sümegi P, Molnár D, Náfrádi K, et al. Vegetation and land snail-based reconstruction of the palaeoecological changes in the forest steppe eco-region of the Carpathian Basin during last glacial warming. *Glob Ecol Conserv.* 2022;33(December 2021):e01976. doi:[10.1016/j.gecco.2021.e01976](https://doi.org/10.1016/j.gecco.2021.e01976)
83. Ludwig P, Gavrilov MB, Radaković MG, Marković SB. Malaco temperature reconstructions and numerical simulation of environmental conditions in the southeastern Carpathian Basin during the last glacial maximum. *J Quat Sci.* 2021;36(8):1426-1435. doi:[10.1002/jqs.3318](https://doi.org/10.1002/jqs.3318)
84. Kovács J, Moravcová M, Újvári G, Pintér AG. Reconstructing the paleoenvironment of east Central Europe in the Late Pleistocene using the oxygen and carbon isotopic signal of tooth in large mammal remains. *Quat Int.* 2012;276-277:145-154. doi:[10.1016/j.quaint.2012.04.009](https://doi.org/10.1016/j.quaint.2012.04.009)
85. Strandberg G, Brandefelt J, Kjellström E, Smith B. High-resolution regional simulation of last glacial maximum climate in Europe. *Tellus Dyn Meteorol Oceanogr.* 2011;63(1):107-125. doi:[10.1111/j.1600-0870.2010.00485.x](https://doi.org/10.1111/j.1600-0870.2010.00485.x)
86. Zepner L, Karrasch P, Wiemann F, Bernard L. ClimateCharts.net – an interactive climate analysis web platform. *Int J Digit Earth.* 2021; 14(3):338-356. doi:[10.1080/17538947.2020.1829112](https://doi.org/10.1080/17538947.2020.1829112)
87. Sümegi P, Magyari E, Dániel P, Molnár M, Töröcsik T. Responses of terrestrial ecosystems to Dansgaard-Oeschger cycles and Heinrich events: A 28,000-year record of environmental changes from SE Hungary. *Quat Int.* 2013;293:34-50. doi:[10.1016/j.quaint.2012.07.032](https://doi.org/10.1016/j.quaint.2012.07.032)
88. Fricke HC, O'Neil JR. The correlation between 18O/16O ratios of meteoric water and surface temperature: its use in investigating terrestrial climate change over geologic time. *Earth Planet Sci Lett.* 1999; 170(3):181-196. doi:[10.1016/S0012-821X\(99\)00105-3](https://doi.org/10.1016/S0012-821X(99)00105-3)
89. Stute M, Forster M, Frischkorn H, et al. Cooling of tropical Brazil (5°C) during the last glacial maximum. *Science.* 1995;269(5222):379-383. doi:[10.1126/science.269.5222.379](https://doi.org/10.1126/science.269.5222.379)
90. Stute M, Schlosser P. Atmospheric Noble Gases. In: *Environmental tracers in subsurface hydrology*. Springer; 2000:349-377. doi:[10.1007/978-1-4615-4557-6_11](https://doi.org/10.1007/978-1-4615-4557-6_11)
91. Cey BD. On the accuracy of noble gas recharge temperatures as a paleoclimate proxy. *J Geophys Res.* 2009;114(D4):D04107. doi:[10.1029/2008JD010438](https://doi.org/10.1029/2008JD010438)
92. Stadelmaier KH, Ludwig P, Bertran P, et al. A new perspective on permafrost boundaries in France during the last glacial maximum. *Clim Past.* 2021;17(6):2559-2576. doi:[10.5194/cp-17-2559-2021](https://doi.org/10.5194/cp-17-2559-2021)
93. Bertran P, Stadelmaier KH, Ludwig P. Last glacial maximum active layer thickness in Western Europe, and the issue of 'tundra gleys' in loess sequences. *J Quat Sci.* 2022;37(7):1222-1228. doi:[10.1002/jqs.3434](https://doi.org/10.1002/jqs.3434)

SUPPORTING INFORMATION

Additional supporting information can be found online in the Supporting Information section at the end of this article.

How to cite this article: Farkas B, Sipos G, Bartyik T, et al. Characterization and mapping of MIS-2 thermal contraction crack polygons in Western Transdanubia, Hungary. *Permafrost and Periglacial Processes.* 2023;34(3):417-427. doi:[10.1002/ppp.2190](https://doi.org/10.1002/ppp.2190)